

LJMU Research Online

Fisher, A, Seaborne, RA, Hughes, TM, Gutteridge, A, Stewart, CE, Coulson, JM, Sharples, AP and Jarvis, JC

Transcriptomic and Epigenetic Regulation of Disuse Atrophy and the Return to Activity in Skeletal Muscle

<http://researchonline.ljmu.ac.uk/id/eprint/6956/>

Article

Citation (please note it is advisable to refer to the publisher's version if you intend to cite from this work)

Fisher, A, Seaborne, RA, Hughes, TM, Gutteridge, A, Stewart, CE, Coulson, JM, Sharples, AP and Jarvis, JC (2017) Transcriptomic and Epigenetic Regulation of Disuse Atrophy and the Return to Activity in Skeletal Muscle. FASEB Journal. Epub A. ISSN 1530-6860

LJMU has developed **LJMU Research Online** for users to access the research output of the University more effectively. Copyright © and Moral Rights for the papers on this site are retained by the individual authors and/or other copyright owners. Users may download and/or print one copy of any article(s) in LJMU Research Online to facilitate their private study or for non-commercial research. You may not engage in further distribution of the material or use it for any profit-making activities or any commercial gain.

The version presented here may differ from the published version or from the version of the record. Please see the repository URL above for details on accessing the published version and note that access may require a subscription.

For more information please contact researchonline@ljmu.ac.uk

<http://researchonline.ljmu.ac.uk/>

Transcriptomic and epigenetic regulation of disuse atrophy and the return to activity in skeletal muscle

Andrew G. Fisher,^{*,1} Robert A. Seaborne,^{†,‡,1} Thomas M. Hughes,[§] Alex Gutteridge,[¶] Claire Stewart,[†] Judy M. Coulson,^{||} Adam P. Sharples,^{†,‡,2} and Jonathan C. Jarvis^{‡,3}

^{*}Institute for Ageing and Chronic Disease and ^{||}Department of Cellular and Molecular Physiology, Institute of Translational Medicine, University of Liverpool, Liverpool, United Kingdom; [†]Institute for Science and Technology in Medicine, Keele University Medical School, Keele University, Staffordshire, United Kingdom; [‡]Stem Cells, Ageing and Molecular Physiology Research Unit, Exercise Metabolism and Adaptation Research Group, Research Institute for Sport and Exercise Sciences, Liverpool John Moores University, Liverpool, United Kingdom; [§]Instituto de Física y Astronomía, Universidad de Valparaíso, Valparaíso, Chile; and [¶]Pfizer, Tadworth, United Kingdom

ABSTRACT: Physical inactivity and disuse are major contributors to age-related muscle loss. Denervation of skeletal muscle has been previously used as a model with which to investigate muscle atrophy following disuse. Although gene regulatory networks that control skeletal muscle atrophy after denervation have been established, the transcriptome in response to the recovery of muscle after disuse and the associated epigenetic mechanisms that may function to modulate gene expression during skeletal muscle atrophy or recovery have yet to be investigated. We report that silencing the tibialis anterior muscle in rats with tetrodotoxin (TTX)—administered to the common peroneal nerve—resulted in reductions in muscle mass of 7, 29, and 51% with corresponding reductions in muscle fiber cross-sectional area of 18, 42, and 69% after 3, 7, and 14 d of TTX, respectively. Of importance, 7 d of recovery, during which rodents resumed habitual physical activity, restored muscle mass from a reduction of 51% after 14 d TTX to a reduction of only 24% compared with sham control. Returning muscle mass to levels observed at 7 d TTX administration (29% reduction). Transcriptome-wide analysis demonstrated that 3714 genes were differentially expressed across all conditions at a significance of $P \leq 0.001$ after disuse-induced atrophy. Of interest, after 7 d of recovery, the expression of genes that were most changed during TTX had returned to that of the sham control. The 20 most differentially expressed genes after microarray analysis were identified across all conditions and were cross-referenced with the most frequently occurring differentially expressed genes between conditions. This gene subset included myogenin (MyoG), Hdac4, Ampd3, Trim63 (MuRF1), and acetylcholine receptor subunit $\alpha 1$ (Chrna1). Transcript expression of these genes and Fbxo32 (MAFbx), because of its previously identified role in disuse atrophy together with Trim63 (MuRF1), were confirmed by real-time quantitative RT-PCR, and DNA methylation of their promoter regions was analyzed by PCR and pyrosequencing. MyoG, Trim63 (MuRF1), Fbxo32 (MAFbx), and Chrna1 demonstrated significantly decreased DNA methylation at key time points after disuse-induced atrophy that corresponded with significantly increased gene expression. Of importance, after TTX cessation and 7 d of recovery, there was a marked increase in the DNA methylation profiles of Trim63 (MuRF1) and Chrna1 back to control levels. This also corresponded with the return of gene expression in the recovery group back to baseline expression observed in sham-operated controls. To our knowledge, this is the first study to demonstrate that skeletal muscle atrophy in response to disuse is accompanied by dynamic epigenetic modifications that are associated with alterations in gene expression, and that these epigenetic modifications and gene expression profiles are reversible after skeletal muscle returns to normal activity.—Fisher, A. G., Seaborne, R. A., Hughes, T. M., Gutteridge, A., Stewart, C., Coulson, J. M., Sharples, A. P., Jarvis, J. C. Transcriptomic and epigenetic regulation of disuse atrophy and the return to activity in skeletal muscle. *FASEB J.* 31, 000–000 (2017). www.fasebj.org

ABBREVIATIONS: Chrna1, acetylcholine receptor subunit $\alpha 1$; CSA, cross-sectional area; DNMT, *de novo* methyltransferase; dNTP, deoxynucleotide; Hdac4, histone deacetylase 4; HRM-PCR, high-resolution melt PCR; MyoG, myogenin; nAChR, nicotinic acetylcholine receptor; qRT-PCR, quantitative RT-PCR; TA, tibialis anterior; TAC, Transcriptome Analysis Console; TTX, tetrodotoxin

¹ These authors contributed equally to this work.

² Correspondence: Institute for Science and Technology in Medicine, Keele University, Guy Hilton Research Centre, Thornburrow Dr., Staffordshire ST4 7QB, United Kingdom. E-mail: a.p.sharples@gmail.com

³ Correspondence: Research Institute for Sport and Exercise Sciences, Liverpool John Moores University, Byrom St. Campus, Liverpool L3 3AF, United Kingdom. E-mail: J.C.Jarvis@ljmu.ac.uk

doi: 10.1096/fj.201700089RR

This article includes supplemental data. Please visit <http://www.fasebj.org> to obtain this information.

Skeletal muscle is the most abundant tissue in the mammalian body and, therefore, maintenance of its structure and function are important to health across the lifespan. The global maintenance of skeletal muscle mass is governed by a fine balance between muscle protein synthesis and degradation. Skeletal muscle undergoes rapid loss—atrophy—during disuse and inactivity (1–4); catabolic/inflammatory disease states, such as cancer cachexia (5, 6), sepsis (7), chronic heart failure (8), and obesity (9); as well as with denervation after, for example, spinal cord injury (10) or during aging (sarcopenia) (11). To investigate the underlying time course and mechanisms of skeletal muscle atrophy, such models as denervation *via* nerve section (12), tetrodotoxin (TTX) injection (13), limb suspension (14), spaceflight (15), and chronic overuse (16, 17) have been implemented. Within these models, large alterations in gene regulatory networks may orchestrate the altered balance between protein synthesis and degradation during muscle wasting (18). Under such conditions, these regulatory networks are altered to favor the breakdown of skeletal muscle proteins, predominantly *via* the ubiquitin-proteasome pathway (19–21). Whereas gene regulatory networks that control skeletal muscle atrophy have been somewhat elucidated, the role of epigenetic alterations in modulating gene expression during skeletal muscle atrophy has received less attention. Furthermore, there are few studies that have investigated the transcriptomic and epigenetic change that underlies the recovery of skeletal muscle after a return to normal physical activity after a period of disuse.

Epigenetic control of gene expression occurs primarily as a result of the modification to DNA or chromatin/histones as well as post-transcriptional modification of RNA (22). It has recently been suggested that denervation-induced atrophy results in the differential expression of genes that are associated with chromatin remodeling (23). Recent *in vitro* evidence also suggests that epigenetic mechanisms may influence regeneration and myotube atrophy (24). Skeletal muscle cells that have encountered the atrophic stimulus of the inflammatory cytokine, TNF- α , during their early proliferative life are more susceptible to TNF- α later in their proliferative life, and demonstrate impaired differentiation and regeneration compared with matched, untreated controls (24). Of importance, in this study, a retention of DNA methylation of the myogenic regulatory factor, MyoD was evident over 30 population doublings in muscle cells that receive a single acute (24-h) cytokine stress in early life (24). This study, therefore, points to a potentially important epigenetic mechanism that underlies the susceptibility to loss of muscle mass (25). Furthermore, recent studies that investigated 44 muscle-specific genes reported that where low methylation occurred, gene enhancer activity increased (26). Despite this, it has not been confirmed *in vivo* whether the modulation of gene expression *via* DNA methylation is a mechanism that regulates skeletal muscle disuse atrophy.

In the present study, we used TTX to silence the nerve to evoke disuse-induced muscle atrophy. TTX inhibits the firing of action potentials by binding to the voltage-gated sodium channel in nerve cell membranes, which blocks the throughput of sodium ions; therefore, the muscles that are

innervated by the blocked nerve cannot be activated to contract (27). This model has the advantage over nerve section in that TTX causes a complete, but reversible, block of sodium channels and, thus, reversible nerve and muscle inactivity. In this study, to investigate both disuse and recovery, TTX was delivered over a preset period after which normal nerve activity resumed. After nerve silencing, DNA microarray technology was used to investigate the temporal genome-wide transcript expression profiles associated with progressive atrophy at 3, 7, and 14 d of disuse. Nerve block was then released, habitual activity resumed, and gene expression profiles were monitored after 7 d of recovery. Finally, DNA methylation within the promoter regions of genes was measured *via* pyrosequencing for genes that demonstrated *via* microarray and confirmatory real-time quantitative RT-PCR (qRT-PCR)—the most significant alterations in expression across all conditions and that were most frequently differentially expressed across all pairwise comparisons. The aim of this investigation was, therefore, to elucidate the epigenetic control of gene expression after disuse atrophy and a return to normal physical activity in skeletal muscle. We hypothesized that disuse atrophy would be controlled by differential DNA methylation and corresponding changes in gene expression, and that these alterations perhaps would be transient and dynamic in nature and, therefore, reversible as normal muscle activity resumes.

MATERIALS AND METHODS

Animals

Ethics approval was obtained and experimental procedures were conducted with the permissions within a project license granted under the British Home Office Animals (Scientific Procedures) Act 1986. Male Wistar rats that weighed between 350–450 g were housed in controlled conditions of 20°C and 45% relative humidity, with food and water available *ad libitum*. Animals were assigned to 5 groups that included 1 control group and 3 TTX-exposed groups for periods of 3, 7, and 14 d, including a 14-d TTX exposure plus 7-d active recovery group. Experimental groups are detailed below and represented schematically in Fig. 1.

Experimental groups

The left common peroneal nerve was exposed to TTX over preset time courses. Groups ($n = 6$) consisted of 3, 7, and 14-d TTX exposure and 14 d of TTX followed by 7 d of natural active recovery. To control TTX exposure, a miniosmotic pump (Mini Osmotic Pump 2002; Alzet, Cupertino, CA, USA) was implanted subcutaneously in the scapular region of animals under TTX conditions. Delivery tubes were subcutaneously channeled to a silicone rubber cuff that was carefully placed around the common peroneal nerve of the left hind limb. Implantation was performed in-house as a modification of a published design (28). The osmotic pump efficiently delivered 0.5 μ l/h TTX (350 μ g/ml in sterile 0.9% saline) to the nerve cuff, which allowed the common peroneal nerve to be exposed to TTX so that the ankle dorsiflexor muscles—tibialis anterior (TA) and extensor digitorum longus—were silenced but normal voluntary plantarflexion was maintained. The general welfare and mobility of group-housed rats were minimally affected. Correct assembly and loading of the osmotic pump and nerve cuff was planned so

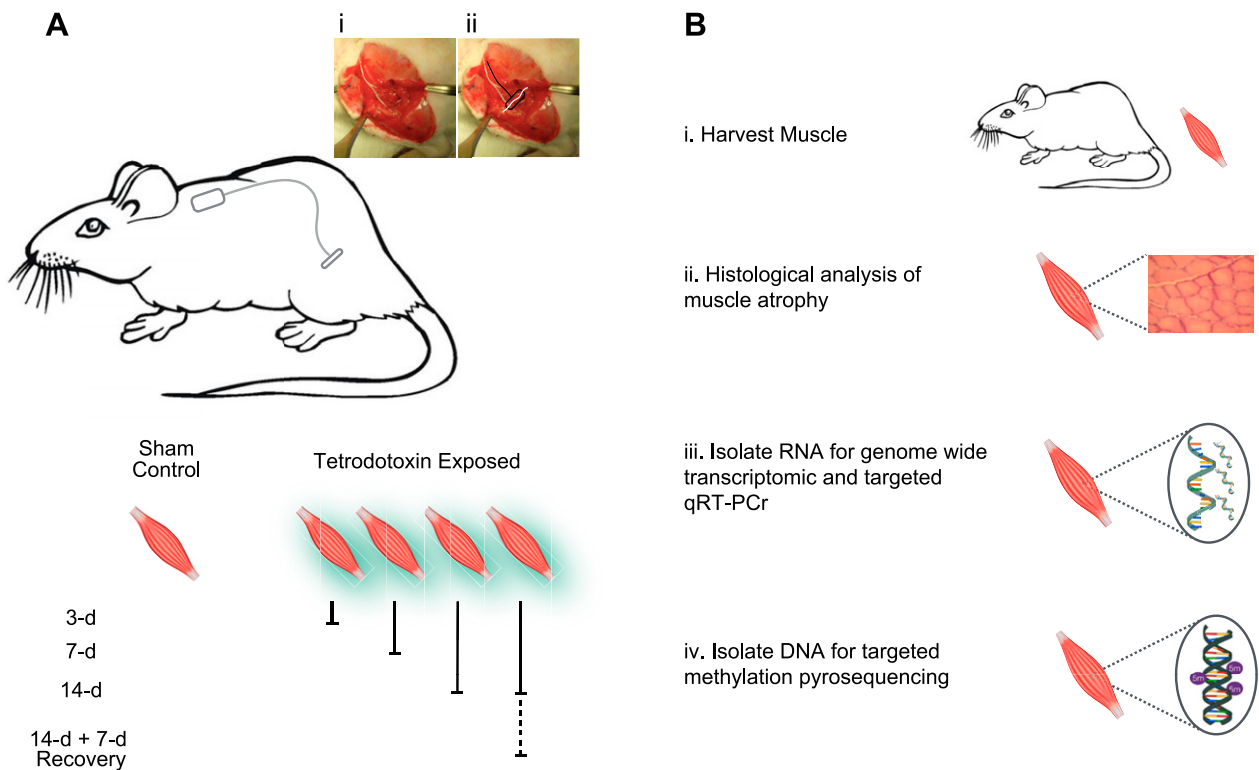


Figure 1. Schematic representation of the TTX muscle atrophy model and subsequent muscle sample preparation for morphologic, transcriptomic, and epigenetic analysis. *A*) Display of physiologic location of TTX administration pump. Real image of osmotic pump location and assembly within the left hindlimb of the rodent (*i*), and a representation overview of the osmotic pump assembly (*ii*; black lines show osmotic pump unit and delivery tube to nerve cuff unit and white line displays the synaptic nerve). *B*) Muscle sample preparation for downstream analysis: treated (left) and untreated contralateral control (right; $n = 6$).

that TTX administration would terminate after 14 d, which allowed the recovery of hindlimb function from d 14 to 21 within the 14-d TTX + 7-d recovery group.

Morphology and histology for muscle size (mass and cross-sectional area)

At the end of each experimental time course, all animals were humanely euthanized with increasing CO₂ concentration and cervical dislocation. For morphologic and histologic purposes, muscle was harvested from control and experimental groups ($n = 6$), weighed, and divided into pieces, and a transverse portion from the midbelly of the muscle was frozen in melting isopentane, cryostat sectioned ($\sim 10 \mu\text{m}$), and stained with hematoxylin and eosin. For each muscle sample, 5 images were obtained at random. By using ImageJ 1.45i software (National Institutes of Health, Bethesda, MD, USA), each photograph was overlaid with an 8×8 grid with which to make an unbiased selection of fibers. Ten fibers were selected for counting for each field of view at the first 10 intersections of the grid that fell within a fiber. Magnification of each section was calibrated from an image of a stage graticule. Cross-sectional area (CSA) was estimated from precise diameter measurements that were taken by selecting 2 points across the minimum diameter and assuming a circular cross-section. Mean TA mass for all control and experimental groups was expressed as a percentage of whole animal body mass ($428 \pm 45 \text{ g}$) to normalize for interindividual differences in animal size ($n = 6$). Mean CSA of TA muscle fiber was expressed as percent change from the untreated contralateral

control limb for each animal ($n = 6$). All data are presented as means \pm SD, unless otherwise stated.

Transcriptome analysis

We conducted microarray analyses to compare genome-wide transcript expression from 3-, 7-, 14-d TTX and 14-d TTX + 7-d recovery ($n = 4$ for each group). Untreated control samples were also used for quality control of microarray analysis and were excluded from the final analysis. Frozen muscle samples were sent to AROS Applied Biotechnology (Aarhus, Denmark), where RNA was isolated *via* AROS Standard Operating Procedures. More than 30,000 rat transcripts and 28,000 variants were examined *via* Affymetrix GeneChip Rat Genome 230 2.0 Array (Affymetrix, High Wycombe, United Kingdom). Raw data files (CEL) were normalized *via* the MAS 5.0 signal method (29, 30), and CHP files were subsequently analyzed for significantly differential gene expression from microarray data [Transcriptome Analysis Console (TAC); Affymetrix]. TAC software was used to create hierarchical clustering heatmaps of the most differentially expressed genes.

RNA isolation and primer design for real-time qRT-PCR

RNA was extracted from frozen muscle tissue ($n = 6$ for all sample groups) and frozen in RNA storage solution (Qiagen, Manchester, United Kingdom). Samples ($\sim 20 \text{ mg}$) were immersed and homogenized in Trizol (Thermo Fischer Scientific, Waltham,

MA, USA), and RNA was extracted according to the manufacturer's instructions. Quantities and quality of RNA were assessed by 260/280 UV spectroscopy (Thermo Fisher Scientific). Isolated RNA produced an average 260/280 ratio of 1.99 (\pm 0.02). Primers were designed with Primer-Basic Local Alignment Search Tool (BLAST) (National Center for Biotechnology Information, Bethesda, MD, USA). All designed primers were between 20 and 21 bp in length and, where possible, had a guanine-cytosine content of 50–55%. The software program, netprimer, predicted the efficiency of the primer products, estimating the probability of primer dimer or hairpin formation. Primers were manufactured by Sigma-Aldrich (St. Louis, MO, USA) and resuspended in either Tris-EDTA buffer or RNA-free water (Sigma-Aldrich) as a 100- μ M stock suspension. Details of primer assays are provided in Table 1.

Real-time qRT-PCR

Real-time qRT-PCR was performed by using either HotStart Taq Master Mix Kit (Qiagen) and an iQ5 Thermocycler (Bio-Rad, Hercules, CA, USA) or QuantiFast SYBR Green RT-PCR one-step kit on a Rotorgene 3000Q (Qiagen). cDNA synthesis for subsequent PCR on the iQ5 Thermocycler was performed as follows: 1 μ g RNA was diluted in 12 μ l of RNA-free water, and 1 μ l of oligo dT primer (Thermo Fisher Scientific) was incubated at 70°C for 10 min and subsequently snap-cooled on ice to enable binding of the primer. A reaction mix—4 μ l of 5 \times buffer, 2 μ l DTT, 1 μ l deoxynucleotides (dNTPs)—were added per RNA sample and incubated at 42°C for 2 min. One microliter of Superscript II Reverse Transcriptase (Thermo Fisher Scientific) was then added and the reaction mix was incubated for an additional 50 min at 42°C. This reaction was inhibited by then heating to 70°C for 15 min. As a control, reactions were prepared in parallel with those previously described for each RNA sample, without the inclusion of the reverse-transcriptase enzyme so that mRNA would not be reverse transcribed into cDNA. These negative control primers were used to confirm that the products amplified by PCR were indeed derived from cDNA. For real-time qPCR using HotStart Taq Master Mix Kit on the iQ5 Thermocycler, reactions were as follows: 3 μ l cDNA, 15 μ l Hotstar Taq Master Mix, and 1.5 μ l each of forward and reverse primer and 9 μ l of RNase-free water, totaling 30 μ l for reactions. For real-time qPCR using QuantiFast SYBR Green RT-PCR One-Step Kit on a Rotorgene 3000Q, reactions were as follows: 9.5 μ l RNA sample (7.3 ng/ μ l = 70 ng total RNA in the reaction), 0.15 μ l of forward primer, 0.15 μ l of reverse primer, 0.20 μ l of reverse transcriptase mix, and 10 μ l of SYBR Green buffer (QuantiFast SYBR Green RT-PCR One-Step Kit; Qiagen), totaling 20 μ l. For the QuantiFast SYBR Green RT-PCR One-Step Kit, reverse transcription cycles were performed in the same tube/reaction before PCR as follows: hold 50°C for 10 min (reverse transcription/cDNA synthesis), followed by 95°C for 5 min (transcriptase inactivation and initial denaturation step), before 40 PCR cycles of 95°C for 10 s (denaturation) and

60°C for 30 s (annealing and extension). Finally, melt curve analyses were performed to identify any primer dimer formation or nonspecific amplification. All melt curves produced single reproducible melt temperatures across all experimental samples. All relative mRNA expression was quantified by using the C_t ($\Delta\Delta C_t$) method (31) against a known reference gene, RPIIb (polr2b) and/or Rn18s. Average C_t values for RPIIb and Rn18s were 20.08 (\pm 0.59) and 15.80 (\pm 0.39), respectively, across all experimental conditions.

DNA isolation and bisulfite conversion

To elucidate methylation profiles, DNA was extracted from frozen muscle tissue by using a commercially available DNA isolation kit (DNA Blood and Muscle Kit; Qiagen) according to manufacturer instructions. For methylation analysis *via* high-resolution melt PCR (HRM-PCR), bisulfite conversion of 2 μ g DNA was performed by using InnuConvert All-in-One Bisulfite Conversion kits (AJ Innuscreen GmbH, Berlin, Germany). For DNA methylation by PCR and pyrosequencing (see Materials and Methods), 500 ng DNA was bisulfite converted by using a Zymo Research EZ Methylation Kit (Zymo Research, Irvine, CA, USA).

DNA methylation by PCR and pyrosequencing

Assays for pyrosequencing were purchased from epigenDX (Hopkinton, MA, USA; summarized in Fig. 2 and Table 2). After bisulfite conversion, PCR reactions were designed depending on the specific DNA methylated region of interest and the size of the product as per the manufacturer's instructions; however, a typical reaction was performed as follows: 3 μ l of 10 \times PCR buffer (containing 15 mM MgCl₂), 0.2 μ l of 10 mM dNTPs, 1.8 μ l of 25 mM MgCl₂, 0.6 μ l of 10 mM dNTPs, 0.15 μ l HotStar Taq Polymerase, 1 μ l of bisulfite-treated DNA, and 0.2 μ M of forward and reverse primer (Table 2). One primer was biotin-labeled and HPLC-purified to facilitate the purification of the final PCR product using Sepharose beads. After an initial denaturation incubation at 95°C for 15 min, 45 cycles of denaturation at 95°C for 30 s, 63°C for 30 s (annealing), and 68°C for 30 s (extension) were performed, with all PCR cycles followed by a final 5 min at 68°C. PCR products were then bound to Streptavidin Sepharose HP (GE Healthcare Life Sciences, Waukesha, WI, USA), after which the immobilized PCR products were purified, washed, denatured with a 0.2- μ M NaOH solution, and rewashed using the Pyrosequencing Vacuum Prep Tool (Qiagen) as per manufacturer instructions. After annealing with 0.5 μ M sequencing primer, purified single-stranded PCR products were sequenced by using the PSQ96 HS System (Qiagen) according to manufacturer instructions. The methylation status of each CpG site was determined individually as an artificial C/T single-nucleotide polymorphism using QCpG software (Qiagen). The methylation

TABLE 1. Primer assay design for real-time qRT-PCR

Gene	Accession No.	Primer, 5'–3'		Primer length (bp)	Optimum annealing temperature (°C)	Product length (bp)
		Forward	Reverse			
<i>Trim63</i>	NM_080903	GGAGGAGTTTACTGAAGAGG	GACACACTTCCCTATGGTGC	20	61	180
<i>Fbxo32</i>	NM_133521	CTTGCTGTGACAAAGGGCAGC	TGAAAGTGAGACGGAGCAGC	20	61	184
<i>Ampd3</i>	NM_031544	ACGCTTGCTGGTCGGTTTAG	TGGCTTCCTTCTGTCCGATG	20	60	197
<i>Hdac4</i>	XM_343629.4	GCAGCCAAACTTCTCCAGCA	TTGACATTGAAACCCACGCC	20	61	212
<i>MyoG</i>	NM_017115.2	GCCATCCAGTACATTGAGCG	CATATCCTCCACCGTGATGC	20	61	267
<i>Chrna1</i>	NM_024485.1	TGTCATCAACACACACCACC	CTGCAATGTACTTCACACCC	20	61	269

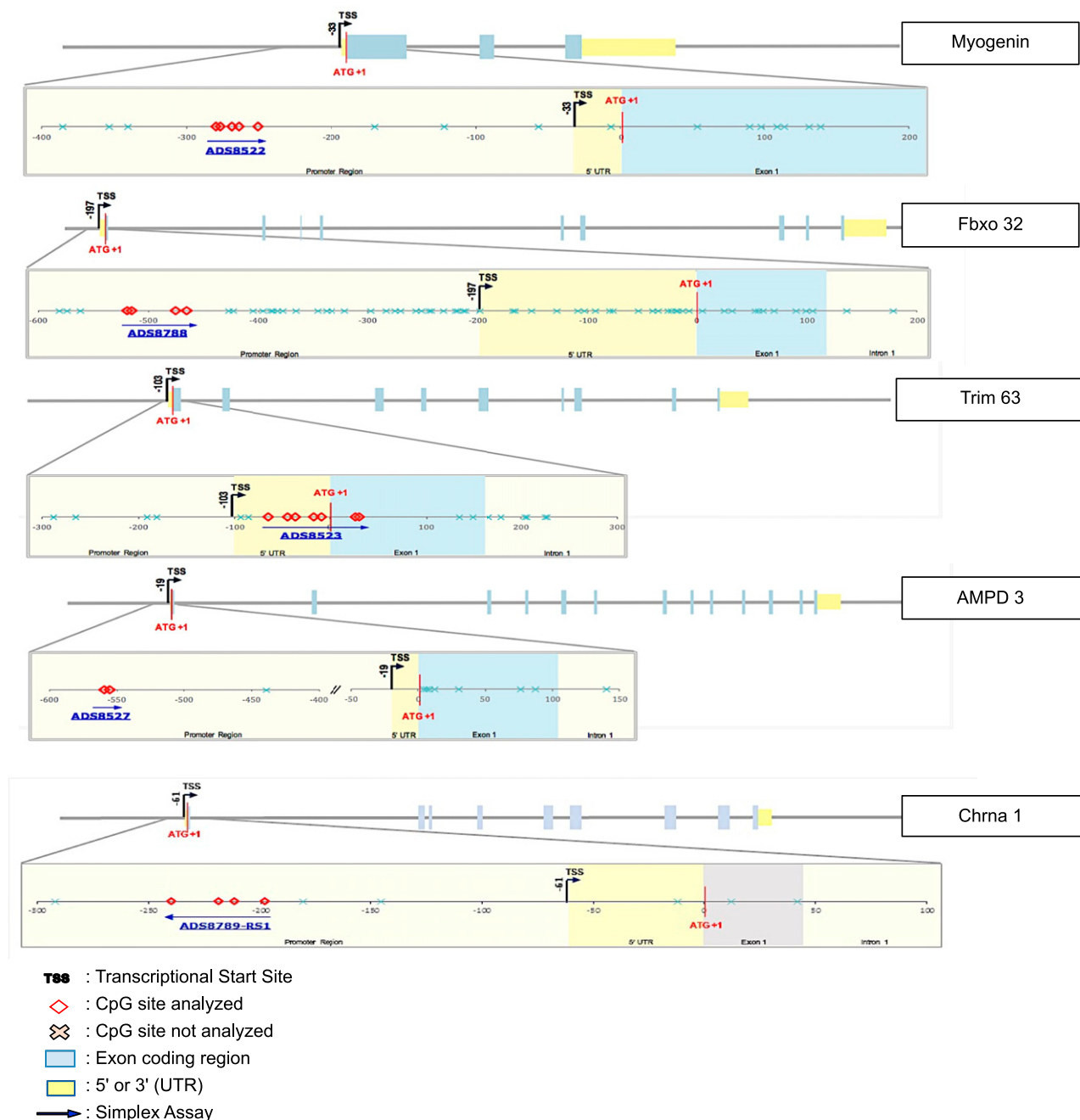


Figure 2. Gene map of CpG islands for loci-specific pyrosequencing for quantification of DNA methylation *via* pyrosequencing. In descending order: MyoG, Fbxo32 (MAFbx), Trim63 (MuRF1), Ampd3, and Chrna1. URT, untranslated region.

level at each CpG site was calculated as the percentage of methylated alleles divided by the sum of all methylated and unmethylated alleles. The mean methylation level was calculated by using the methylation levels of all measured CpG sites within the targeted region of each gene. Each experiment included non-CpG cytosines as internal control to detect the incomplete bisulfite conversion of the input DNA. In addition, a series of unmethylated and methylated DNA strands were included as a control after each PCR. Furthermore, PCR bias testing was performed by mixing unmethylated control DNA with *in vitro* methylated DNA at different ratios (0, 5, 10, 25, 50, 75, and 100%), followed by bisulfite modification, PCR, and pyrosequencing analysis. All supporting information for gene assays, including assay sequence, chromosomal CpG island locations, position from the ATG start

codon and transcriptional start site, and CpG number are given in Fig. 2 and Table 2.

HRM-PCR for total DNA methylation

HRM-PCR for CpG methylation was performed as previously described (24). In brief, 20 ng DNA was subjected to HRM-PCR using EpiTect HRM-PCR kits and Rotorgene 3000Q (Qiagen) with Rotorgene software. All primer concentrations for gene CpG assays and EpiTect HRM master mix volumes were used in accordance with manufacturer instructions. HDAC4 (Qiagen) was designed to amplify a product length of 140–190 bp (Table 3). PCR cycles were performed as follows: 10 s at 95°C (denaturation), 30 s at 55°C (annealing), and 10 s at 72°C

TABLE 2. Description of targeted DNA methylation assays for loci-specific pyrosequencing analysis

Gene	CpG	Position from ATG codon	Position from TSS	Chromatin location	Sequence to analyze
<i>MyoG</i>	CpG-9	-280 to -251	-247 to -218	Chr13: 51126212-51126241	AGTYGAYGGTTTTTTTGTGTTATAGGAGTYGTTTGGG
	CpG-8	-280	-247	Chr13: 51126212	
	CpG-7	-277	-244	Chr13: 51126215	
	CpG-6	-269	-236	Chr13: 51126223	
	CpG-5	-264	-231	Chr13: 51126228	
<i>Trim63</i>		-251	-218	Chr13: 51126241	ATTGAGTGGGATTTTTTTTATTTGGTGTGAYTAGGTGG AAGAGATAGTYGTAGTTTGAAGTAATATGGATTATAA ATTTGGTTTGATTTYGGAYGGAATG
		-63 to +30	+40 to +133	Chr5: 152533388-152533481	
	CpG-5	-64	40	Chr5: 152533388	
	CpG-4	-44	60	Chr5: 152533408	
	CpG-3	-36	68	Chr5: 152533416	
<i>Ampld3</i>	CpG-2	-17	87	Chr5: 152533435	GYGGYGTATGGGTG
	CpG-1	-9	95	Chr5: 152533443	
	CpG1	26	129	Chr5: 152533447	
	CpG2	30	133	Chr5: 152533481	
	CpG-10	-559 to -555	-540 to -536	Chr1: 175585557-175585561	
<i>Flxo32</i>	CpG-9	-559	-540	Chr1: 175585557	TAYGTTYGATAGGGGAGTAGGGGAGGTGTAAAGAGGTGTTA GGGTATYGAGGGTTAGYGGGATATTTCG
		-555	-536	Chr1: 175585561	
		-519 to -465	-322 to -268	Chr7: 98098536-98098590	
	CpG-49	-519	-322	Chr7: 98098590	
	CpG-48	-515	-318	Chr7: 98098586	
<i>Chna1</i>	CpG-47	-475	-278	Chr7: 98098546	TCTACTCATATTAACRTAAACCRATATAAAAACTACATA AATCRTAAACCAAAAAAC
	CpG-46	-465	-268	Chr7: 98098536	
		-198 to -240	-137 to -179	Chr3: 60460861-60460903	
	CpG-7	-240	-179	Chr3: 60460903	
	CpG-6	-219	-158	Chr3: 60460882	
	CpG-5	-212	-151	Chr3: 60460875	
	CpG-4	-198	-137	Chr3: 60460861	

TSS, transcription start site.

TABLE 3. *HDAC4* DNA methylation via HRM-PCR

Gene	CpG no.	GeneGlobe no.	Chromatin location	Sequence to analyze	Product length (bp)
<i>Hdac4</i>	1	PM00599046	Chr9: 91389151–91391341	GGGCGCGCAAGAGCGCAGACTGTGAC GGGGGCCCCGT	190
	2	PM00599053	Chr9: 91390077–91391147	GCGCCCGCGAAGCGGGGTGGCTGTT GGGCTATTGTAGGGCGGA	138
	3	PM00599060	Chr9: 91389052–91391220	GCTAGCGCCTGGAGAGTCCTCGGTAC GCCCCGC	168
	4	PM00599067	Chr9: 91389477–91391621	GCTTTGGGTCGCCGCCACCGCGTCCC GGT	144
	5	PM00599074	Chr9: 91389472–91391621	CGTTGCTGTGGCGGAGGTGTAGGCTT TGGGTCGCCGCCACCGCGTCCCG	149

(extension) for a maximum of 55 cycles. After PCR, an HRM analysis was performed with 0.1°C increments from 65°C to 95°C. Fluorescence *vs.* melt temperature was used to create a standard curve using rat methylated DNA standards that represented 100, 75, 50, 25, 10, 5, and 0% methylation. All samples were run in duplicate and were normalized to 0% methylated control and averaged to produce a single curve. The relationship between the area under the curve—determined *via* each standard curve—and the corresponding percentage methylation curve of specific gene loci was determined by using the best-fitting fourth-order polynomial relation. This relationship was subsequently used to quantify the percent methylation from the integrated raw melt curves of the experimental samples. Calculations were performed by using a Python-based program, MethylCal, that was developed for this purpose in-house [used previously (24)].

Statistical analyses

All statistical analyses of morphologic data were performed *via* either R software (v.2.13.1; <http://www.R-project.org>) or SPSS (v.22.0; SPSS, Chicago, IL, USA). Morphologic (muscle mass and CSA) comparisons between experimental and control conditions were assessed *via* 1-way between-group ANOVA. Microarray data were analyzed for statistical comparisons *via* 1-way between-group ANOVA within the TAC software. Targeted real-time qRT-PCR was analyzed by using a 1-way between-group ANOVA (with Tukey's *post hoc* tests). DNA methylation data sets were analyzed by using a 2-way between-group ANOVA (with Tukey's *post hoc* tests), which allowed comparison of experimental conditions and individual CpG islands. A follow-up 1-way ANOVA between CpG islands at each experimental condition was used to identify significant differences in the DNA methylation status of each CpG island within the same experimental condition. Finally, Student's *t* tests were used to identify significant differences in CpG methylation between experimental conditions and control. All statistical analyses for DNA methylation were performed on absolute values, with figures representing data as mean \pm SD to relevant control. Differences were considered statistically significant at values of $P \leq 0.05$.

RESULTS

Skeletal muscle disuse and recovery evokes considerable, yet reversible, muscle atrophy

Exposure to TTX produced an average of $7.0 \pm 2.4\%$ loss in TA muscle mass at 3 d, $28.7 \pm 5.1\%$ at 7 d, and $50.7 \pm 2.7\%$ loss after 14 d that resulted in statistical significance at all

time points *vs.* the unoperated right TA ($P < 0.001$; Fig. 3) and a significant difference between paired comparisons of 3 and 7 d, 3 and 14 d, 7 and 14 d ($P < 0.001$). After 14 d of TTX exposure followed by 7 d of cessation in the recovery group, muscle mass significantly recovered by 51.7% *vs.* 14 d of denervation ($P = 0.001$; Fig. 3). Seven days of recovery did not completely restore muscle mass, as muscle mass was still significantly lower than control ($P < 0.001$; Fig. 3), and total muscle mass was equivalent to levels at 7 d of TTX administration, which suggests that rates of loss over 7 d were similar to rates of recovery. We therefore report significant skeletal muscle atrophy of the TA muscles with disuse and a 51.7% recovery of muscle mass after 7 d of cessation of TTX administration and the return of normal habitual physical activity *vs.* 14 d of TTX induced-denervation.

Exposure to TTX produced a progressive reduction in mean muscle fiber CSA of $17.95 \pm 12.06\%$ at 3 d, $42.09 \pm 6.17\%$ at 7 d, and $68.94 \pm 2.97\%$ at 14 d of TTX exposure, with 7 and 14 d of TTX being significantly reduced *vs.* control ($P = 0.003$ and $P < 0.001$, respectively; Fig. 4). Similar to TA muscle mass, upon TTX cessation, the 14-d TTX + 7-d recovery group muscle CSA significantly recovered compared with 14 d of TTX alone, with an increase of 62.6% in CSA compared with 14 d of TTX alone ($P = 0.002$; Fig. 4); therefore, there was significant atrophy of individual skeletal muscle fibers in TA muscles after denervation, and a 51.7% recovery of muscle mass and a 62.6% recovery of muscle CSA after 7 d of cessation of TTX administration and a return to normal habitual physical activity.

Gene expression microarrays identify important gene regulatory networks involved in muscle atrophy and recovery

After confirming a significant reduction in muscle mass, the temporal transcriptome profile that accompanied muscle atrophy was investigated ($n = 4$). The dendrogram from the hierarchical clustering of probe sets across the genome identified 3714 genes that demonstrated highly significant differential expression across all conditions with a value of $P \leq 0.001$ (Fig. 5A). It also demonstrated that there was high clustering similarity for the 3-, 7-, and 14-d TTX groups, which were dissimilar to the sham-operated controls and the recovery group that also

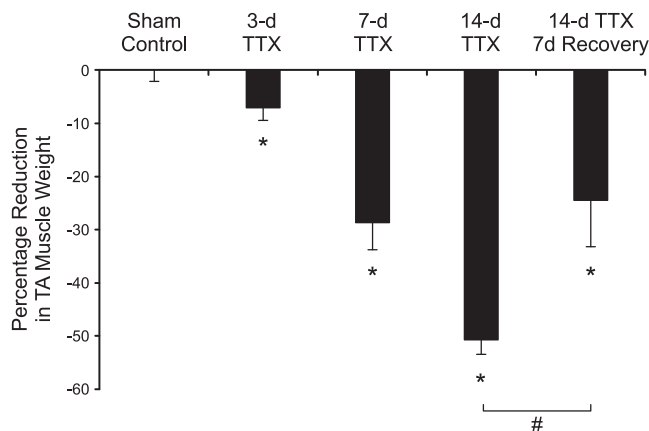


Figure 3. Quantification of muscle atrophy (muscle mass) *in vivo* after TTX-induced nerve block. Data shown for 3, 7, and 14 d of treatment, and TTX nerve block + 7 d of active recovery (7-d Recovery). Mean TA mass for all control and experimental groups were expressed as a percentage difference of whole-animal body mass (428 ± 45 g) to normalize for interindividual differences in animal size. All data are presented as means \pm SD for $n = 6$ in each condition. *Statistically significant *vs.* sham control ($P < 0.05$); #statistically significant *vs.* 14-d TTX ($P < 0.05$).

demonstrated high clustering similarity (Fig. 5A and Supplemental 1A). This suggested that disuse-induced atrophy evoked a considerable change in the expression of a large number of genes that were returned to levels similar to those in sham controls on the cessation of nerve block in the recovery group (Fig. 5A). Despite the top 20 genes showing recovery to control sham levels, 846 genes were still significantly differentially expressed ($P < 0.05$) in the recovery group compared with sham control (Supplemental 1I). Additional analyses were performed by using unsupervised hierarchical clustering of the top 20 most differentially expressed genes (Fig. 5B and Supplemental 2). This analysis confirmed that these top 20 genes that were most differentially expressed in TTX groups returned to sham control after 7 d of recovery. Furthermore, the top 500 genes that were up-regulated by TTX administration could be grouped into 3 distinct clusters on the basis of their temporal behavior: an immediate and sustained increase in expression (Fig. 5C), a delayed, but progressive, increase in expression (Fig. 5D), and, finally, an immediate increase in expression that declined over the time course (Fig. 5E), which suggested that dynamic and coordinated gene expression occurred across a large number of genes as a result of disuse, and that there was a return to control levels in the recovery group.

Regulated genes identified by microarray and ranked by significance of change

Transcriptome-wide data were analyzed to compare conditions in 6 pairwise comparisons [sham *vs.* 3 d (Supplemental 1C), 7 d (Supplemental 1D), and 14 d (Supplemental 1E); and Recovery *vs.* 3 d (Supplemental 1F), 7 d (Supplemental 1G), and 14 d (Supplemental 1H)] to identify the genes that were among the most significantly affected in the experimental

groups. Trim 63 (MuRF1), myogenin (MyoG), and Ampd3 were identified as being the most frequently occurring genes that were most differentially expressed across these paired comparisons and that also appeared in the top 20 differentially expressed genes across all conditions (Fig. 5B and Supplemental 1B). Ampd3 appeared in 4 of 6 of these paired comparisons (Supplemental 1C, F–H). Previous studies have also suggested that overexpression of Ampd3 increases protein degradation in C2C12 myotubes (32); therefore, we sought to further elucidate its transcriptional and epigenetic role in denervation-induced atrophy in the present study. The E3 ubiquitin ligase, Trim63, appeared in 3 of 6 paired comparisons (Supplemental 1C, F, H) and has been previously strongly associated with muscle atrophy *in vitro* and *in vivo* (33–37), as has been its protein family member, Fbxo32 (Mafbx). We therefore extended the analysis of this change by qRT-PCR and loci-specific pyrosequencing for the role of DNA methylation in TTX-induced atrophy and recovery. The muscle-specific basic helix-loop-helix myogenic regulatory factor, MyoG, was also identified in 3 of 6 paired comparisons (Supplemental Fig. 1C–E) and has previously been identified as a key transcript in the regulation of denervation-dependent muscular atrophy in rodent models (38). Of importance, the class II histone deacetylase 4 (Hdac4) also appeared within the top 20 most statistically differentially expressed genes across all probe sets (Fig. 5B and Supplemental 1B) and was the most statistically differentially expressed gene when comparing sham control with 3-d TTX atrophy probe sets (Supplemental 1C). Hdac4 is a known upstream regulatory factor of MyoG activity (36, 39), and, thus, both Hdac4 and MyoG genes were identified as warranting additional targeted analysis. Additionally, a neuromuscular junction-associated gene that was significantly altered and that also appeared in the top 20 most differentially expressed genes included the acetylcholine receptor subunit $\alpha 1$ (Chrna1; Fig. 5B). This gene also appeared in 2 of 6 paired comparisons of most differentially expressed genes (Supplemental 1D, E). Chrna1 plays a crucial role in acetylcholine binding and the channel-gating activity within the neuromuscular junction pathway (40) and has been previously been identified *via* transcriptome analysis as the most differentially expressed gene in skeletal muscle loss observed in age-related muscle loss/denervation (41). After the identification of key gene transcripts, quantification of gene expression was elucidated *via* follow-up real-time qRT-PCR to confirm and further profile the transcriptional responses, and DNA methylation analyses were performed *via* pyrosequencing to assess the DNA methylation status of the gene promoter region in response to disuse-induced muscle atrophy and recovery.

Changes in gene expression after disuse-induced atrophy are returned to control levels after recovery

Confirmation of microarray gene expression by qRT-PCR demonstrated that MyoG, Hdac4, Trim63, and Fbxo32 were significantly increased at 3 d of TTX exposure compared with control ($P < 0.05$), with Hdac4 and Fbxo32

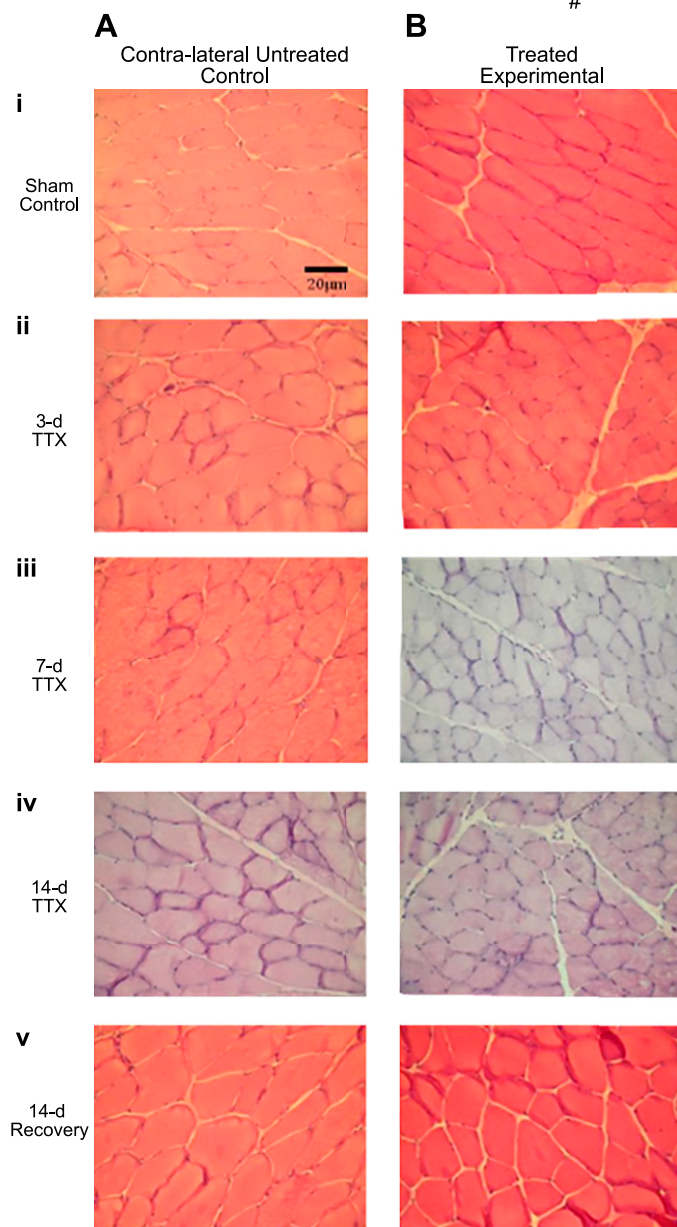
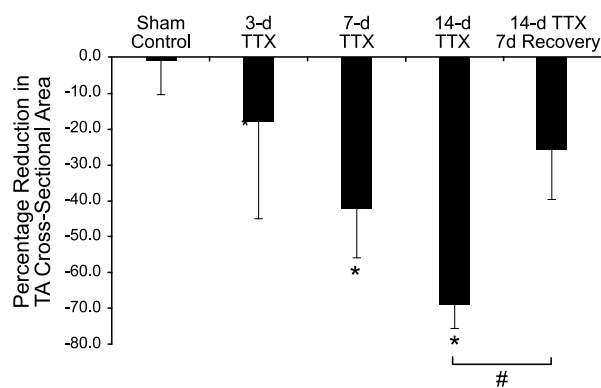
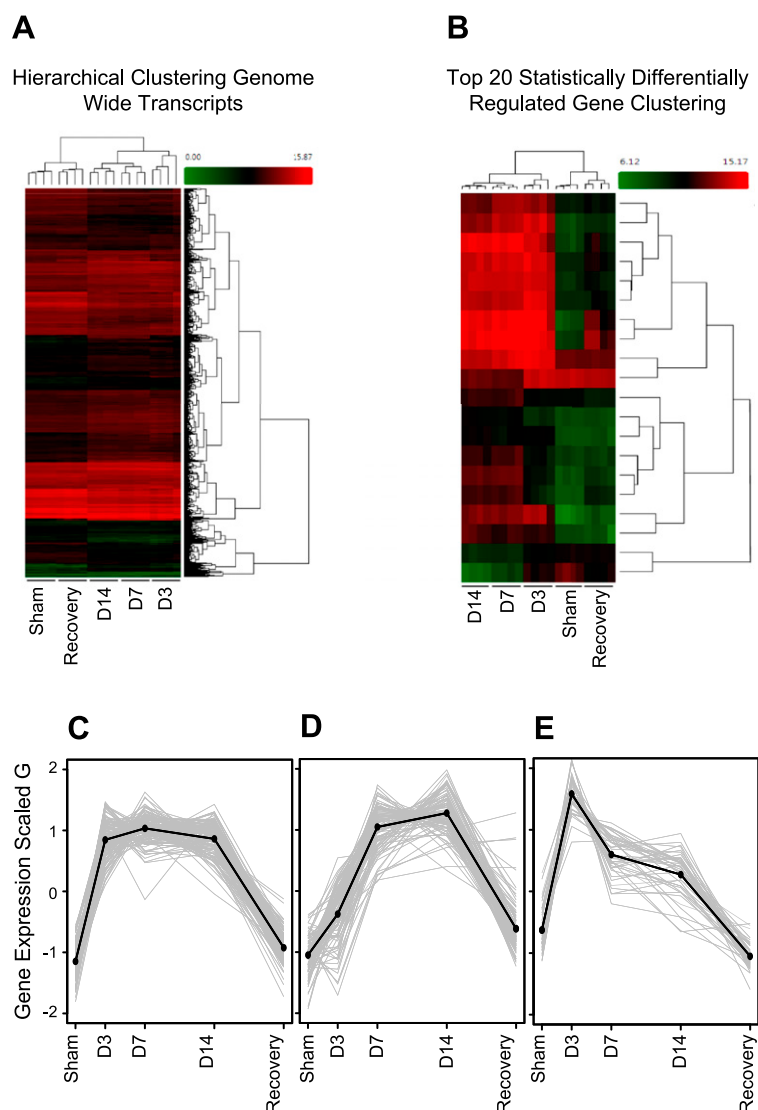


Figure 4. Muscle fiber CSA after TTX-induced atrophy and recovery. Mean CSA of the TA muscle was expressed as a percent change from untreated contralateral control limb for each animal. *A, B* Hematoxylin and eosin-stained sections of untreated (*A*) and treated (*B*) TA muscle of control (*i*), 3-d TTX exposed (*ii*), 7-d TTX exposed (*iii*), 14-d TTX exposed (*iv*), and 14-d TTX exposed with 7-d recovery (*v*). *Statistically significant *vs.* sham control ($P < 0.05$); #statistically significant *vs.* 14-d TTX ($P < 0.05$).

(Fig. 6A) remaining elevated at 7 d of TTX exposure. By 14 d, mean levels for Hdac4, MyoG, Trim63, and Fbxo32 were not significantly different, that suggested an elevation of these genes at 3 and 7 d in response to disuse. In contrast, whereas significant changes in Ampd3 expression were not detected (Fig. 6A), Chrna1 expression was significantly

elevated at 3, 7, and 14 d (177.5-fold increase *vs.* control; $P = 0.016$; Fig. 6A). After TTX cessation and 7 d of recovery, it was also confirmed *via* qRT-PCR that Hdac4, MyoG, Trim63, Fbxo32, and Chrna1 gene expression had all returned to sham control levels, as demonstrated in the microarray data.

Figure 5. Transcriptome analysis indicated a highly dynamic gene expression response to progressive muscular atrophy that returns to expression levels in the sham control upon muscle recovery. *A*) Hierarchical clustering heatmaps of probe set expression across the rodent genome identified 3714 genes that were highly statistically significantly ($P \leq 0.001$) expressed across all conditions, with 3-, 7-, and 14-d TTX atrophy being differentially expressed compared with sham control and 14-d TTX + 7-d recovery. *B*) This observation was confirmed in analysis of the top 20 statistically differentially expressed genes across all conditions. Similar clustering occurred within 3-, 7-, and 14-d of TTX exposure which was distinctly dissimilar to the clustering observed in the sham control and 7-day recovery group. *C–E*) Top 500 most statistically differentially expressed genes grouped into 3 distinct temporal expression patterns: an immediate and sustained increase in expression (*C*); delayed, but progressive, increase in expression (*D*); or an immediate increase in expression that declined over the time course (*E*). Of note, all gene clusterings return to sham control expression levels upon TTX cessation and 7 d of recovery.



Changes in DNA methylation were associated with altered gene expression in disuse-induced atrophy and recovery

Loci-specific pyrosequencing of individual CpG islands within gene promoters revealed significant alterations in the DNA methylation of key genes that were identified after microarray analysis and confirmatory real-time qRT-PCR that corresponded with significant increases in gene transcription. After 3 d of TTX exposure, there was a significant reduction ($P = 0.011$) of DNA methylation in the *MyoG* gene promoter (Fig. 6B) and a concomitant significant increase ($P = 0.011$) in *MyoG* gene expression (Fig. 6A), both of which then returned to baseline levels during the remaining 14 d (all gene expression/DNA methylation overlap relationships are schematically represented in Fig. 6C). The DNA methylation profile of the *Chrna1* gene promoter progressively decreased relative to control, with 7 and 14 d of TTX treatment attaining significance compared with sham control ($P = 0.035$ and $P < 0.001$, respectively). This corresponded with the increased expression of this gene over the 14-d denervation period

(Fig. 6A, C). As with *Chrna1*, *Trim63* displayed a significant reduction in methylation at 7 and 14 d of TTX exposure ($P = 0.035$ and $P < 0.001$, respectively; Fig. 6B, C), which coincided with a stable increase in mRNA expression at the same time points (Fig. 6A, C). *Fbxo32* demonstrated a decreasing trend in DNA methylation at specific time points, attaining significance at 14 d of TTX exposure ($P = 0.021$; Fig. 6B, C), with gene expression data demonstrating significant increases at 3 ($P = 0.037$) and 7 d ($P = 0.038$) atrophy (Fig. 6A, C). Of importance, after TTX cessation, there was recovery in the DNA methylation profiles of *Trim63*, *Fbxo32*, and *Chrna1*, which returned to sham control levels ($P > 0.05$). This was in conjunction with an observed recovery of gene expression of the same genes upon TTX cessation (Fig. 6C). We observed no differences in DNA methylation for *Ampd3* after TTX administration or recovery (Fig. 6B). Furthermore, after initial total percent of methylation within the total amplicon/product *via* HRM-PCR for *Hdac4*, we were unable to identify methylation greater than that of the 0% methylation control for all conditions, and, therefore, pyrosequencing for loci-specific DNA methylation was not performed for *Hdac4*.

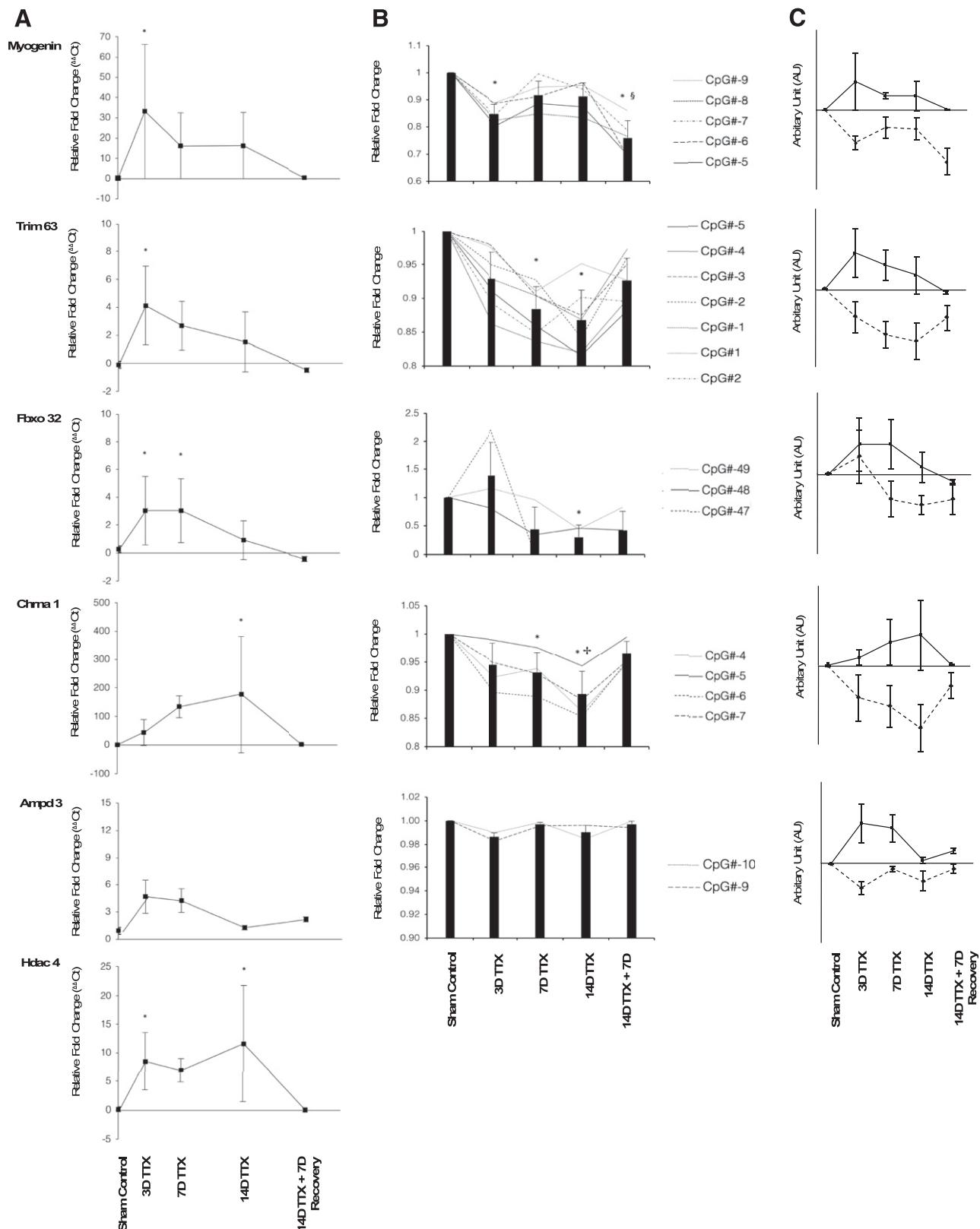


Figure 6. Relative fold change of gene expression and DNA methylation of a subset of identified gene transcripts. A) Relative fold change in mRNA expression of genes MyoG, Trim63, Fbxo32, Chrna1, Ampd3, and Hdac4 (in descending order). All genes are presented as means \pm SD ($n = 6$), Ampd3 ($n = 3$). Statistically significant changes in fold difference compared with sham control group are indicated *via* *. Sham control group is represented with triangle icon. All TTX-treated groups are represented with a square icon. B) Mean methylation data presented as relative fold change compared with sham control for genes: MyoG, Trim63, Fbxo32, Chrna1, and Ampd3 (in descending order). Mean percentage data (black column bars) are the average taken from each CpG island of the respective gene, analyzed *via* loci-specific pyrosequencing. Individual CpG island methylation percentages are (continued on next page)

DISCUSSION

Summary

The aim of this investigation was to elucidate the epigenetic control of gene expression after skeletal muscle disuse-induced atrophy after 3, 7, and 14 d of nerve block with TTX. First, we observed a 7, 29, and 51% loss of muscle at 3, 7, and 14 d of disuse, with 7 d of recovery resulting in a 51.7% restoration of total muscle mass that had been lost after 14 d of disuse. Muscle mass was therefore similar after 7 d of disuse or 14 d of disuse followed by 7 d of normal activity. Muscle atrophy was further confirmed with fiber cross-sectional area data in which a similar pattern of progressive loss of 18, 42, and 69% was observed after 3, 7, and 14 d of TTX, respectively. Seven days of recovery restored 63% of muscle cross-sectional area *vs.* 14 d of disuse-induced atrophy alone. Our original hypothesis was supported, in that disuse-induced atrophy was associated with reduced DNA methylation and enhanced gene expression. Both DNA methylation and gene expression were partially returned to baseline after 7 d of recovery from nerve block. Of importance, after gene expression microarray analysis, we found that 3714 genes were significantly differentially regulated ($P \leq 0.001$) across all TTX groups, and that these genes were returned in the recovery group to levels that were observed in sham control. Specifically, by identifying the top 20 most differentially expressed genes in the atrophy and recovery groups and cross-referencing with the most frequently occurring significantly regulated genes for between-group pairwise comparisons, we identified a key subset of influential genes: MyoG, Hdac4, Trim63 (Murf1), Ampd3, and Chrna1. These genes—together with Fbxo32 (Mafbx), because of its previously defined role with Trim63 (Murf1) in muscle atrophy—were then analyzed *via* real-time qRT-PCR to confirm microarray gene expression data for these genes as well as loci-specific DNA methylation of the promoter regions by pyrosequencing. All of these genes—MyoG, Hdac4, Trim63/Murf1, Ampd3, Chrna1, and Fbxo32/Mafbx—have been identified previously *via* transcriptome-wide analysis of disuse-induced atrophy after neuromuscular blocker α -cobrotoxin treatment (42). In this investigation, we have identified novel data that suggest that MyoG, Trim63 (Murf1), Fbxo32 (Mafbx), and Chrna1 demonstrate reduced DNA methylation at specific time points after disuse-induced atrophy that corresponded with increases in gene expression at the same time points. Of importance, after TTX cessation and 7 d of recovery, during which normal habitual physical activity was resumed, there was a return of DNA methylation for Trim63, Fbxo32, and Chrna1 to sham control levels. This also corresponded

with the return of gene expression to that of baseline sham control levels. Because the reduced DNA methylation within promoter or enhancer regions of genes can lead to enhanced gene expression as a result of reduced methylation, which allows access for RNA polymerase to enable transcription (43), our data suggest that atrophy and recovery of skeletal muscle after disuse is associated with dynamic and transient epigenetic modifications that correspond with altered gene expression.

Dynamic and transient DNA methylation after atrophy and recovery of muscle mass

Interestingly, 51.7% of total muscle mass loss after 14 d was restored after 7 d of recovery, yet, importantly, gene expression was returned fully to baseline after 7 d, which suggests—as perhaps would be expected because of the time required for transcription, translation, and protein incorporation—a time lag between gene expression and the physiological restoration of muscle mass. The findings in this study, however, suggest that reduced DNA methylation that corresponded with increased gene expression of MyoG, Trim63 (Murf1), Fbxo32 (Mafbx), and Chrna1 are dynamic and transient events, in which decreases in DNA methylation at 3, 7, and 14 d of TTX-induced atrophy correspond with increases in gene expression that, in turn, are returned to baseline (Trim63/Murf1 and Chrna1) within just 7 d after the removal of the TTX block. DNA methylation has previously been reported to be mitotically stable and, as such, environmental factors were previously believed to be unable to induce significant alterations in DNA methylation at both acute and chronic time points (44). Furthermore, our previous data suggest that even after acute catabolic stress, DNA methylation can be stably retained across several population doublings of muscle cells *in vitro* (24); however, we demonstrate here that DNA methylation does respond at a rate that allows for its participation in the adaptive control of gene expression and therefore adds additional weight to previous findings in support of transient alterations of DNA methylation in skeletal muscle, for example, as previously after an acute bout of aerobic exercise (24, 45). Our data therefore add support to previous findings demonstrating transient alterations of skeletal muscle DNA methylation.

Although not identified in this study, it will be important in future studies to investigate DNA methyltransferase activity. The DNA methyltransferases (DNMT3a/3b) are involved in the initial incorporation of methyl groups to cytosine residues and the creation of 5-methylcytosine to increase DNA methylation. Maintenance DNA methyltransferase (DNMT1) is involved in retaining the methyl tag on the DNA strand (46). The dynamic and transient observation of DNA methylation in this study is perhaps

visualized as individual lines. DNA methylation data presented as means \pm SD for $n = 3$. *Statistically significant reductions compared with the sham control group; [§]significant reduction compared with 7- and 14-d TTX atrophy; [†]significant reduction in DNA methylation compared with 3-d TTX-exposed experimental group (B). C) An overlap schematic represents the relationship between DNA methylation and mRNA expression of key transcripts (arbitrary units). bHLH muscle specific basic helix-loop-helix; H&E, hematoxylin and eosin; MRF, myogenic regulatory factor.

suggestive of high DNMT3a/3b activity in which initial and rapid increases in DNA methylation are observed; however, we do not report a significant retention of DNA methylation upon TTX cessation (14-d TTX + 7-d recovery), which would perhaps suggest that DNMT1 did not maintain the methylation status of some of these genes during muscle recovery. It has previously been reported that increases in both types of DNMT are observed after a high-fat diet that induces increases in DNA methylation of 6508 genes (47). Additional work is needed to confirm similar findings in atrophying muscle and to elucidate the response of DNA methyltransferases upon the reversible insult. Finally, it would be important to undertake 14 d of recovery in future experiments to assess whether muscle mass can be returned fully to baseline control levels and to examine the transcriptomic and epigenetic responses during this period.

DNA methylation correlates with important changes in skeletal muscle gene expression after disuse-induced atrophy and with the return of gene expression to baseline during recovery

As suggested above, MyoG, Trim63, Fbxo32, and Chrna1 demonstrated decreased DNA methylation after disuse-induced atrophy that corresponded with increased gene expression. Of importance, after TTX cessation and 7 d of recovery, during which normal habitual physical activity was resumed, DNA methylation of Trim63 and Chrna1 returned to sham control levels as the suppressed levels of gene expression recovered. The muscle-specific basic helix-loop-helix transcriptional factor and member of the myogenic regulatory factors, MyoG, is commonly associated with the coordination of skeletal muscle development/myogenesis or skeletal muscle regeneration and, specifically, the differentiation/fusion of skeletal muscle cells (48). Here, we report a significant induction of gene expression for this transcription factor upon disuse-induced muscle atrophy. Because expression of this protein is usually associated with muscle regeneration, this may reflect a compensatory mechanism in an unsuccessful attempt to halt atrophy or to respond to a return of activity. The role of MyoG as a transcription factor has previously been linked with the regulation of the ubiquitin E3 ligases, Trim63 and Fbxo32, and associated muscle atrophy (34). We provide novel data that suggest that the DNA methylation profile of this transcript is altered in an inverse fashion to its mRNA expression. Indeed, at 3, 7, and 14 d, we observed a significant reduction in MyoG DNA methylation and an increase in MyoG transcript expression; therefore, we suggest that increased MyoG gene expression is regulated by reduced MyoG DNA methylation.

Previous studies have also reported that MyoG gene expression is under the regulatory control of class II Hdacs (34, 35). In partial support of this notion, we report a significant increase in Hdac4 gene expression at 3 and 14 d of TTX exposure; however, we did not measure protein abundance or the phosphorylation/deacetylation status of Hdac4. Indeed, the initial screening of Hdac4 DNA

methylation *via* HRM-PCR was unable to detect a notable change, with global gene percentage methylation indicating no methylation above 0% methylated controls. Therefore, additional work at the protein and histone levels is needed to elucidate the epigenetic regulation of Hdacs during periods of loss and recovery of muscle mass, as its altered gene expression after denervation does not seem to be controlled *via* DNA methylation. Furthermore, despite a return of MyoG gene expression to control levels after 7 d of recovery, DNA methylation continued to reduce in the recovery group. This suggested that while reduced DNA methylation may have been important in increased gene expression during denervation-induced atrophy, DNA methylation was not controlling the gene expression of MyoG during recovery.

As previously suggested, downstream transcriptional targets of MyoG have also been shown to be highly induced in rodents during periods of muscle loss caused by denervation, immobilization, and unloading (49, 50). Trim63 is an E3 ubiquitin ligase and a member of the RING zinc finger family of proteins that directs the polyubiquitination of proteins to target them for proteolysis. With catabolic stimuli, such as diabetes, cancer, denervation, unloading, and glucocorticoid or cytokine treatment, its expression has consistently been demonstrated to increase (50, 51). Previous studies have also suggested that upon denervation, Northern blot analysis identified a significant increase in Trim63 and Fbxo32 after 3 d of muscle atrophy, that continued through to 7 d (50). Here, we report a significant increase in Trim63 and Fbxo32 gene expression *via* real-time qRT-PCR compared with control levels in parallel with a reduction in DNA methylation. This suggests an important role for epigenetic control of these ubiquitin ligases in the resulting protein degradation and muscle loss that has been observed in this study. We note that DNA methylation of both of these ubiquitin ligases increased to control levels with corresponding decreases in gene expression to the sham control level, which also suggests that the reductions in DNA methylation during atrophy can be dynamically regulated.

Furthermore, Chrna1 makes up the majority of the muscle-specific nicotinic acetyl choline receptor (nAChR) in adult skeletal muscle (52) and plays a crucial role in initiating the opening of the nAChR channels and the transfer of positively charged ions (53). We reported a progressive increase in gene expression resulting in a cumulative significant fold change after 14 d of TTX exposure. This alteration in gene expression was met with a parallel progressive reduction in DNA methylation with significance being observed at both 7 and 14 d after TTX-induced atrophy. An observation similar to previous work (54), in which a significant increase in Chrna1 activity was observed as a result of sarcopenia. nAChRs are made up of 5 isoforms in human skeletal muscle, in which the subunit Chrna1 is most dominant. These isoforms function to create an acetylcholine cluster around the neuromuscular central pore, in which they house target binding sites predominantly located at the α -subunit in the extracellular domain near the N terminus. Upon contact of a chemical messenger to the binding site, all present subunits undergo a conformational change that results in the opening

of the nAChR channel (55). Upon denervation, however, no action potential messages are received and, therefore, it is possible that the reduced DNA methylation and increased transcriptional response—although we do not provide evidence of protein levels—may increase as a compensatory mechanism that is understood to increase the chance of forming new end plates. This response is equivalent to that observed after nerve section and it seems, therefore, to be a response to the lack of activity rather than the physical absence or damage to the nerve. Further, upon TTX cessation and muscle recovery, we report a return of Chrn1 DNA methylation and gene expression back towards sham control levels.

Finally, it is important to note that MyoG, ubiquitin ligases, and Chrn1 have been identified as major regulators of muscle regeneration, protein degradation, and function, respectively, and that the present study identified these genes as being the most frequently occurring, differentially expressed genes across comparisons by using a nonselective transcriptome-wide approach in a novel model of osmotically administered TTX-induced atrophy. Therefore, these data further consolidate the important role for epigenetics in the regulation of these genes in disuse-induced atrophy and the recovery of skeletal muscle following a return to activity.

CONCLUSIONS

MyoG, Trim63, Fbxo32, and Chrn1, but not Ampd3, demonstrate decreased DNA methylation after disuse-induced atrophy that correspond with increased gene expression and muscle atrophy. Importantly, after TTX cessation and 7 d of recovery, there was increased DNA methylation of Trim63 and Chrn1 to control levels that also corresponded with the return of gene expression to that of baseline in sham controls. Overall, this suggests that the atrophy and recovery of skeletal muscle after disuse is controlled by the dynamic and transient epigenetic regulation of gene expression.

FJ

ACKNOWLEDGMENTS

This work was supported by an integrative mammalian biology studentship from the UK Medical Research Council [to A.G.F. (via J.C.J.)], as well as by a Doctoral Training Alliance funded studentship and GlaxoSmithKline [to R.A.S. (via A.P.S.)]. The authors declare no conflicts of interest.

AUTHOR CONTRIBUTIONS

A. G. Fisher, R. A. Seaborne, J. M. Coulson, A. P. Sharples, and J. C. Jarvis designed research; A. G. Fisher, R. A. Seaborne, T. M. Hughes, A. Gutteridge, C. Stewart, J. M. Coulson, A. P. Sharples, and J. C. Jarvis analyzed data; A. G. Fisher, R. A. Seaborne, J. M. Coulson, A. P. Sharples, and J. C. Jarvis performed research; A. G. Fisher, R. A. Seaborne, C. Stewart, A. P. Sharples, and J. C. Jarvis wrote the paper; and T. M. Hughes contributed analytic tools.

REFERENCES

- Ferrando, A. A., Lane, H. W., Stuart, C. A., Davis-Street, J., and Wolfe, R. R. (1996) Prolonged bed rest decreases skeletal muscle and whole body protein synthesis. *Am. J. Physiol.* **270**, E627–E633
- LeBlanc, A. D., Schneider, V. S., Evans, H. J., Pientok, C., Rowe, R., and Spector, E. (1992) Regional changes in muscle mass following 17 weeks of bed rest. *J. Appl. Physiol.* (1985) **73**, 2172–2178
- Gibson, J. N., Halliday, D., Morrison, W. L., Stoward, P. J., Hornsby, G. A., Watt, P. W., Murdoch, G., and Rennie, M. J. (1987) Decrease in human quadriceps muscle protein turnover consequent upon leg immobilization. *Clin. Sci. (Lond.)* **72**, 503–509
- Deitrick, J. E. (1948) The effect of immobilization on metabolic and physiological functions of normal men. *Bull. N. Y. Acad. Med.* **24**, 364–375
- Acharyya, S., Ladner, K. J., Nelsen, L. L., Damrauer, J., Reiser, P. J., Swoap, S., and Guttridge, D. C. (2004) Cancer cachexia is regulated by selective targeting of skeletal muscle gene products. *J. Clin. Invest.* **114**, 370–378
- Tan, B. H., and Fearon, K. C. (2008) Cachexia: prevalence and impact in medicine. *Curr. Opin. Clin. Nutr. Metab. Care* **11**, 400–407
- Hasselgren, P. O., and Fischer, J. E. (1998) Sepsis: stimulation of energy-dependent protein breakdown resulting in protein loss in skeletal muscle. *World J. Surg.* **22**, 203–208
- Strassburg, S., Springer, J., and Anker, S. D. (2005) Muscle wasting in cardiac cachexia. *Int. J. Biochem. Cell Biol.* **37**, 1938–1947
- Kalyani, R. R., Corriere, M., and Ferrucci, L. (2014) Age-related and disease-related muscle loss: the effect of diabetes, obesity, and other diseases. *Lancet Diabetes Endocrinol.* **2**, 819–829
- Giangregorio, L., and McCartney, N. (2006) Bone loss and muscle atrophy in spinal cord injury: epidemiology, fracture prediction, and rehabilitation strategies. *J. Spinal Cord Med.* **29**, 489–500
- Janssen, I., Heymsfield, S. B., and Ross, R. (2002) Low relative skeletal muscle mass (sarcopenia) in older persons is associated with functional impairment and physical disability. *J. Am. Geriatr. Soc.* **50**, 889–896
- Batt, J., Bain, J., Goncalves, J., Michalski, B., Plant, P., Fahnestock, M., and Woodgett, J. (2006) Differential gene expression profiling of short and long term denervated muscle. *FASEB J.* **20**, 115–117
- Dupont Salter, A. C., Richmond, F. J., and Loeb, G. E. (2003) Effects of muscle immobilization at different lengths on tetrodotoxin-induced disuse atrophy. *IEEE Trans. Neural Syst. Rehabil. Eng.* **11**, 209–217
- De Boer, M. D., Maganaris, C. N., Seynnes, O. R., Rennie, M. J., and Narici, M. V. (2007) Time course of muscular, neural and tendinous adaptations to 23 day unilateral lower-limb suspension in young men. *J. Physiol.* **583**, 1079–1091
- Nikawa, T., Ishidoh, K., Hirasaka, K., Ishihara, I., Ikemoto, M., Kano, M., Kominami, E., Nonaka, I., Ogawa, T., Adams, G. R., Baldwin, K. M., Yasui, N., Kishi, K., and Takeda, S. (2004) Skeletal muscle gene expression in space-flown rats. *FASEB J.* **18**, 522–524
- Jarvis, J. C., and Salmons, S. (1991) A family of neuromuscular stimulators with optical transcutaneous control. *J. Med. Eng. Technol.* **15**, 53–57
- Jarvis, J. C., Mokrusch, T., Kwende, M. M., Sutherland, H., and Salmons, S. (1996) Fast-to-slow transformation in stimulated rat muscle. *Muscle Nerve* **19**, 1469–1475
- Bonaldo, P., and Sandri, M. (2013) Cellular and molecular mechanisms of muscle atrophy. *Dis. Model. Mech.* **6**, 25–39
- Eddins, M. J., Varadan, R., Fushman, D., Pickart, C. M., and Wolberger, C. (2007) Crystal structure and solution NMR studies of Lys48-linked tetraubiquitin at neutral pH. *J. Mol. Biol.* **367**, 204–211
- Sandri, M., Sandri, C., Gilbert, A., Skurk, C., Calabria, E., Picard, A., Walsh, K., Schiaffino, S., Lecker, S. H., and Goldberg, A. L. (2004) Foxo transcription factors induce the atrophy-related ubiquitin ligase atrogin-1 and cause skeletal muscle atrophy. *Cell* **117**, 399–412
- Lecker, S. H., Jagoe, R. T., Gilbert, A., Gomes, M., Baracos, V., Bailey, J., Price, S. R., Mitch, W. E., and Goldberg, A. L. (2004) Multiple types of skeletal muscle atrophy involve a common program of changes in gene expression. *FASEB J.* **18**, 39–51
- Jaenisch, R., and Bird, A. (2003) Epigenetic regulation of gene expression: how the genome integrates intrinsic and environmental signals. *Nat. Genet.* **33** (Suppl), 245–254
- Magnusson, C., Svensson, A., Christerson, U., and Tägerud, S. (2005) Denervation-induced alterations in gene expression in mouse skeletal muscle. *Eur. J. Neurosci.* **21**, 577–580
- Sharples, A. P., Polydorou, I., Hughes, D. C., Owens, D. J., Hughes, T. M., and Stewart, C. E. (2016) Skeletal muscle cells possess a

- 'memory' of acute early life TNF- α exposure: role of epigenetic adaptation. *Biogerontology* **17**, 603–617
25. Sharples, A. P., Stewart, C. E., and Seaborne, R. A. (2016) Does skeletal muscle have an 'epi'-memory? The role of epigenetics in nutritional programming, metabolic disease, aging and exercise. *Aging Cell* **15**, 603–616
 26. Ehrlich, K. C., Paterson, H. L., Lacey, M., and Ehrlich, M. (2016) DNA hypomethylation in intragenic and intergenic enhancer chromatin of muscle-specific genes usually correlates with their expression. *Yale J. Biol. Med.* **89**, 441–455
 27. Buffelli, M., Pasino, E., and Cangiano, A. (1997) Paralysis of rat skeletal muscle equally affects contractile properties as does permanent denervation. *J. Muscle Res. Cell Motil.* **18**, 683–695
 28. Michel, R. N., and Gardiner, P. F. (1990) To what extent is hindlimb suspension a model of disuse? *Muscle Nerve* **13**, 646–653
 29. Irizarry, R. A., Bolstad, B. M., Collin, F., Cope, L. M., Hobbs, B., and Speed, T. P. (2003) Summaries of affymetrix geneChip probe level data. *Nucleic Acids Res.* **31**, e15
 30. Irizarry, R. A., Hobbs, B., Collin, F., Beazer-Barclay, Y. D., Antonellis, K. J., Scherf, U., and Speed, T. P. (2003) Exploration, normalization, and summaries of high density oligonucleotide array probe level data. *Biostatistics* **4**, 249–264
 31. Schmittgen, T. D., and Livak, K. J. (2008) Analyzing real-time PCR data by the comparative C_T method. *Nat. Protoc.* **3**, 1101–1108
 32. Davis, P., Witczak, C., and Brault, J. (2015) AMP deaminase 3 accelerates protein degradation in C2C12 myotubes. *FASEB J.* **29**
 33. Cohen, S., Brault, J. J., Gygi, S. P., Glass, D. J., Valenzuela, D. M., Gartner, C., Latres, E., and Goldberg, A. L. (2009) During muscle atrophy, thick, but not thin, filament components are degraded by MuRF1-dependent ubiquitylation. *J. Cell Biol.* **185**, 1083–1095
 34. Cohen, T. J., Waddell, D. S., Barrientos, T., Lu, Z., Feng, G., Cox, G. A., Bodine, S. C., and Yao, T. P. (2007) The histone deacetylase HDAC4 connects neural activity to muscle transcriptional reprogramming. *J. Biol. Chem.* **282**, 33752–33759
 35. Tang, H., and Goldman, D. (2006) Activity-dependent gene regulation in skeletal muscle is mediated by a histone deacetylase (HDAC)-Dach2-myogenin signal transduction cascade. *Proc. Natl. Acad. Sci. USA* **103**, 16977–16982
 36. Tang, H., Macpherson, P., Marvin, M., Meadows, E., Klein, W. H., Yang, X. J., and Goldman, D. (2009) A histone deacetylase 4/myogenin positive feedback loop coordinates denervation-dependent gene induction and suppression. *Mol. Biol. Cell* **20**, 1120–1131
 37. Tang, W. W., Dietmann, S., Irie, N., Leitch, H. G., Floros, V. I., Bradshaw, C. R., Hackett, J. A., Chinnery, P. F., and Surani, M. A. (2015) A unique gene regulatory network resets the human germline epigenome for development. *Cell* **161**, 1453–1467
 38. Macpherson, P. C. D., Wang, X., and Goldman, D. (2011) Myogenin regulates denervation-dependent muscle atrophy in mouse soleus muscle. *J. Cell. Biochem.* **112**, 2149–2159
 39. Moresi, V., Williams, A. H., Meadows, E., Flynn, J. M., Potthoff, M. J., McAnally, J., Shelton, J. M., Backs, J., Klein, W. H., Richardson, J. A., Bassel-Duby, R., and Olson, E. N. (2010) Myogenin and class II HDACs control neurogenic muscle atrophy by inducing E3 ubiquitin ligases. *Cell* **143**, 35–45
 40. Yu, X. M., and Hall, Z. W. (1991) Extracellular domains mediating epsilon subunit interactions of muscle acetylcholine receptor. *Nature* **352**, 64–67
 41. Ibebunjo, C., Chick, J. M., Kendall, T., Eash, J. K., Li, C., Zhang, Y., Vickers, C., Wu, Z., Clarke, B. A., Shi, J., Cruz, J., Fournier, B., Brachet, S., Gutzwiller, S., Ma, Q., Markovits, J., Broome, M., Steinkrauss, M., Skuba, E., Galarneau, J. R., Gygi, S. P., and Glass, D. J. (2013) Genomic and proteomic profiling reveals reduced mitochondrial function and disruption of the neuromuscular junction driving rat sarcopenia. *Mol. Cell. Biol.* **33**, 194–212
 42. Llano-Diez, M., Gustafson, A.-M., Olsson, C., Goransson, H., and Larsson, L. (2011) Muscle wasting and the temporal gene expression pattern in a novel rat intensive care unit model. *BMC Genomics* **12**, 602
 43. Bogdanović, O., and Veenstra, G. J. (2009) DNA methylation and methyl-CpG binding proteins: developmental requirements and function. *Chromosoma* **118**, 549–565
 44. Reik, W., Dean, W., and Walter, J. (2001) Epigenetic reprogramming in mammalian development. *Science* **293**, 1089–1093
 45. Barrès, R., Yan, J., Egan, B., Treebak, J. T., Rasmussen, M., Fritz, T., Caidahl, K., Krook, A., O'Gorman, D. J., and Zierath, J. R. (2012) Acute exercise remodels promoter methylation in human skeletal muscle. *Cell Metab.* **15**, 405–411
 46. Trasler, J., Deng, L., Melnyk, S., Pogribny, I., Hiou-Tim, F., Sibani, S., Oakes, C., Li, E., James, S. J., and Rozen, R. (2003) Impact of Dnmt1 deficiency, with and without low folate diets, on tumor numbers and DNA methylation in Min mice. *Carcinogenesis* **24**, 39–45
 47. Jacobsen, S. C., Brøns, C., Bork-Jensen, J., Ribel-Madsen, R., Yang, B., Lara, E., Hall, E., Calvanese, V., Nilsson, E., Jørgensen, S. W., Mandrup, S., Ling, C., Fernandez, A. F., Fraga, M. F., Poulsen, P., and Vaag, A. (2012) Effects of short-term high-fat overfeeding on genome-wide DNA methylation in the skeletal muscle of healthy young men. *Diabetologia* **55**, 3341–3349
 48. Le Grand, F., and Rudnicki, M. A. (2007) Skeletal muscle satellite cells and adult myogenesis. *Curr. Opin. Cell Biol.* **19**, 628–633
 49. Bodine, S. C., and Baehr, L. M. (2014) Skeletal muscle atrophy and the E3 ubiquitin ligases MuRF1 and MAFbx/atrogen-1. *Am. J. Physiol. Endocrinol. Metab.* **307**, E469–E484
 50. Bodine, S. C., Latres, E., Baumhueter, S., Lai, V. K., Nunez, L., Clarke, B. A., Poueymirou, W. T., Panaro, F. J., Na, E., Dharmarajan, K., Pan, Z. Q., Valenzuela, D. M., DeChiara, T. M., Stitt, T. N., Yancopoulos, G. D., and Glass, D. J. (2001) Identification of ubiquitin ligases required for skeletal muscle atrophy. *Science* **294**, 1704–1708
 51. Goldberg, A. L. (1969) Protein turnover in skeletal muscle. II. Effects of denervation and cortisone on protein catabolism in skeletal muscle. *J. Biol. Chem.* **244**, 3223–3229
 52. Giniatullin, R., Nistri, A., and Yakel, J. L. (2005) Desensitization of nicotinic ACh receptors: shaping cholinergic signaling. *Trends Neurosci.* **28**, 371–378
 53. Beker, F., Weber, M., Fink, R. H., and Adams, D. J. (2003) Muscarinic and nicotinic ACh receptor activation differentially mobilize Ca^{2+} in rat intracardiac ganglion neurons. *J. Neurophysiol.* **90**, 1956–1964
 54. Ibebunjo, C. (2013) Genomic and proteomic profiling reveals reduced mitochondrial function and disruption of the neuromuscular junction driving rat sarcopenia. *Mol. Cell. Biol.* **33**, 194–212
 55. Colquhoun, D., and Sivilotti, L. G. (2004) Function and structure in glycine receptors and some of their relatives. *Trends Neurosci.* **27**, 337–344

Received for publication March 15, 2017.

Accepted for publication July 25, 2017.

Transcriptomic and epigenetic regulation of disuse atrophy and the return to activity in skeletal muscle

Andrew G. Fisher, Robert A. Seaborne, Thomas M. Hughes, et al.

FASEB J published online August 17, 2017

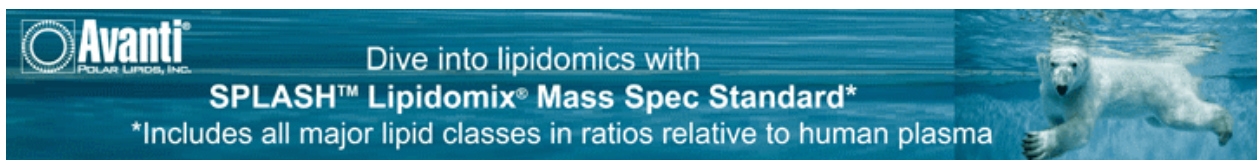
Access the most recent version at doi:[10.1096/fj.201700089RR](https://doi.org/10.1096/fj.201700089RR)

Supplemental Material <http://www.fasebj.org/content/suppl/2017/08/17/fj.201700089RR.DC1>

Subscriptions Information about subscribing to *The FASEB Journal* is online at <http://www.faseb.org/The-FASEB-Journal/Librarian-s-Resources.aspx>

Permissions Submit copyright permission requests at:
<http://www.fasebj.org/site/misc/copyright.xhtml>

Email Alerts Receive free email alerts when new an article cites this article - sign up at <http://www.fasebj.org/cgi/alerts>



Avanti[®]
POLAR LIPIDS, INC.

Dive into lipidomics with
SPLASH[™] Lipidomix[®] Mass Spec Standard*

*Includes all major lipid classes in ratios relative to human plasma